LAMINAR BURNING VELOCITY, MARKSTEIN LENGTH AND CELLULAR INSTABILITY OF SPHERICALLY PROPAGATING NH_3/H_2/AIR PREMIXED FLAMES AT VARIOUS PRESSURES

Huizhen Li [1], Huahua Xiao [1], Jinhua Sun [1]
[1] State Key Laboratory of Fire Science, University of Science and Technology of China, Anhui, China
Email: xiaoh@ustc.edu.cn

ABSTRACT

Blending hydrogen into ammonia can improve the burning intensity of ammonia and the safety of hydrogen, and it is important to understand the flames of NH_3/H_2/air mixtures. In this work, laminar flame characteristics of 50:50 (vol%) ammonia-hydrogen mixtures in air were studied using the spherical flame propagation method in a constant-volume bomb at initial temperature T_u = 298K and different pressures. Laminar burning velocity and Markstein length were evaluated using a linear analysis method. The influences of equivalence ratio ($0.8 \leq \phi \leq 1.4$) and initial pressure (P_u = 0.5 atm, 1.0 atm and 1.5 atm) on flame instability were analyzed by examining the Lewis number, flame thickness, and thermal expansion ratio. The result shows that the laminar burning velocity varies non-monotonically with equivalence ratio and decreases with increasing initial pressure. The Markstein length increases monotonically with the increase of equivalence ratio, but decreases with initial pressure. Flame morphology shows that the ammonia-hydrogen flames suffer from cellular instabilities, especially at higher pressures, i.e., 1.0 and 1.5 atm. The flame stability increases with increasing equivalence ratio and decreases with initial pressure. In addition, numerical calculations show that five commonly-used detailed NH_3/H_2/air mechanisms were not capable of accurately predicting the unstretched flame propagation velocities for the mixtures considered here. Thus, the experimental measurements in this study can be helpful in further improving and validating these reaction mechanisms.

Keywords: Ammonia; Hydrogen; Laminar burning velocity; Markstein length; Cellular instability

1.0 INTRODUCTION

In recent decades, the shortage of fossil fuels and the increasingly greenhouse effect have become more and more serious. Ammonia as a carbon-free and good carrier of hydrogen energy (high hydrogen weight of 17.7% [1]) has attracted many attentions. Compared with hydrogen, ammonia has more advantages in storage and transportation with high boiling temperature (-33.4 ℃ at 1.0atm) and high energy density (12.7MJ/L at -33.4 ℃ and 1.0atm) [2]. Studies show that direct combustion of ammonia as energy has been widely used in many devices, e.g., gas turbine[3], engines[4], and fuel cells [5].

However, there are challenges in using ammonia as fuel alone. The minimum ignition energy of NH_3/air flame is about 680 mJ and higher than CH_4/air (about 0.47mJ) and H_2/air flames (about 0.02mJ). NH_3/air flame has a narrower flammability range with φ =16.5-29 vol% [6] compared to φ =

5-16 vol% for CH_4/air flame [7] and φ = 4.5-75 vol% for H_2/air flame [6]. The laminar burning velocity of NH_3/air flame at atmospheric pressure and room temperature is between 6~8cm/s (equivalence ratio of ϕ = 1.1) [8]. It is much lower than that of hydrocarbon fuel, and the value is almost 1/5 of the CH_4/air flame (about 35cm/s)[9]. Therefore, it is necessary to establish a reasonable scheme that can ensure a more effective combustion of NH_3. Blending ammonia with other fuels is one of the promising options, e.g., CH_4/NH_3/air [10], NH3/syngas/air [2], NH3/dimethyl ether/air [11]. Furthermore, combustion of NH_3/H_2/air mixtures is much more attractive with the beneficial characteristics of no carbon emission, enhancing H_2 safety and improving NH_3 combustion intensity.

The study by Lee et al. [12] shows that the laminar burning velocity has a substantial increase with hydrogen addition for the laminar hydrogen-added ammonia/air flames at atmospheric pressure, particularly under fuel-rich conditions. Ichikawa et al. [13] found that initial pressure has a negative effect on flame propagation speed of ammonia/hydrogen/air mixtures. According to Li et al. [14], the enhancement of the laminar burning velocity with the hydrogen addition is mainly due to chemical effect caused by the reduction in chemical activation energy and the transport effect resulting from the high mobility of hydrogen. When ammonia and hydrogen are burned in equal proportion (50%NH_3/50%H_2/air), the laminar burning velocity is close to that of methane/air flames. Nonetheless, few previous studies specifically analyzed the combustion of 50%NH_3/50%H_2/air mixtures. In addition, many tested mechanisms [2] predicted poorly the laminar burning velocity of ammonia/hydrogen/air flames, especially for high hydrogen ratio addition. This is because these kinetics mechanisms could not be effectively verified due to a lack of experimental data.

This paper is mainly devoted to investigating the 50%NH_3/50%H_2/air laminar flames characteristics at room temperature (298K) and various pressures using a constant-volume-combustion bomb method. In addition, five detailed kinetics mechanisms are selected to evaluate the laminar burning velocity of 50%NH_3/50%H_2/air flames and compared with the experiments.

2.0 Experimental setup and numerical method

The experimental system employed is mainly composed of six parts: a spherical constant-volume-combustion chamber, a gas premixing chamber, a high-speed schlieren cinematography system, a pressure recording system, a high-voltage ignition system, and a synchronization controller, shown schematically in Figure 1. The volume of the combustion chamber is 4.2 L with an inner diameter of 200 mm. Two 80 mm diameter quartz optical windows are oppositely mounted. The schlieren system adopts a way of linear transmission-type layout. The high-speed camera is operated at 10000 fps. The pressure inside the chamber during flame propagation is measured using a pressure transducer (Kistler 601CAA) and HICORDER (HIOKI, MEMORY HICORDER 8826). The mixture is ignited by spark electrodes in the center of the chamber. The pressure recorder, high-speed camera, and spark igniter are controlled by the synchronization system.

The mixture is prepared according to Dalton's law of partial pressure. The intake quantity of ammonia (purity 99.999%), hydrogen (purity 99.999%) and synthetic air (21%O_2/79%N_2 99.999%) are controlled using the static absloute pressure transmitters (claimed accuracy of 0.15% of reading). Each test was repeated at least three times in the experiment.

Numerical simulations in this study were performed using premixed module of CHEMKIN-PRO [15], a one-dimensional freely propagating laminar flame model. Thermal diffusion (Soret effect) and multicomponent transportation were taken into account in the simulations. For each case, at least 500 grid points were used with CRUV 0.03 and CRAD 0.03. Five mechanisms were used to calculate the unstretched laminar burning velocity and compare with the experimental results obtained in this work, i.e., Mei-Mech [16], Han-Mech [17], Dagaut-Mech [18], Nakamura-Mech [19] and Zhang-Mech [20].

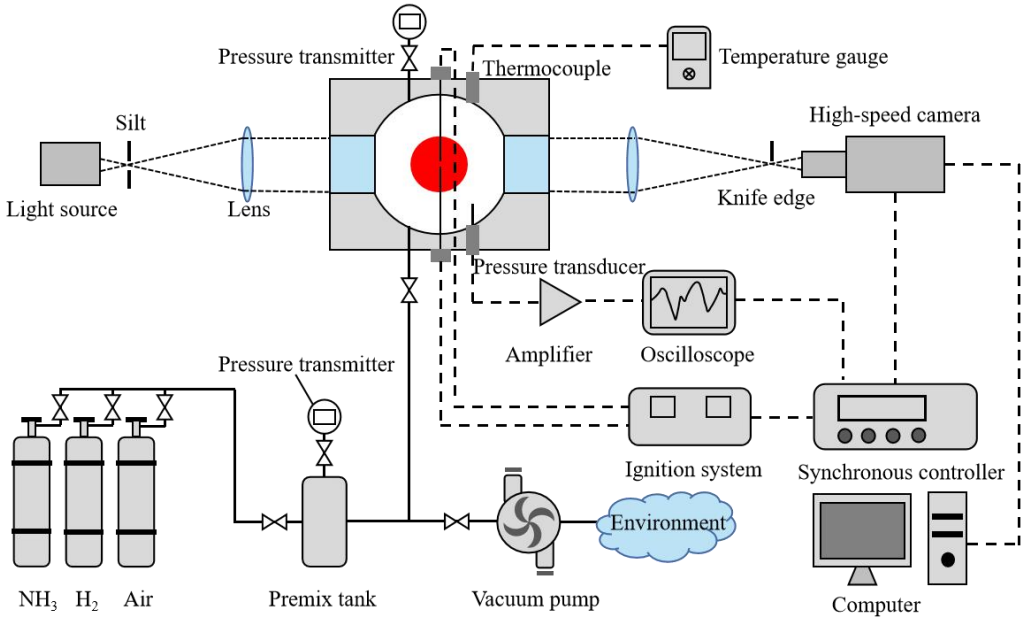

Figure 1. Schematic of the experimental apparatus.

3.0 PARAMETER EVALUATION METHOD

3.1 Laminar burning velocity and Markstein length

The laminar burning velocity and Markstein length are obtained as follows. To avoid the influence of ignition process, the initial radius in present work was chosen to be 6 mm [21]. The upper radius limit is 30 mm (about 0.3 times the radius of the wall [22]) and the effect of the chamber can be neglected.

The stretched flame propagation speed, S_b , was derived from the data of flame radius versus time:

$$S_b = \frac{dR}{dt} \tag{1}$$

Where R- flame radius, mm; t-time, s. The flame stretch rate, κ, is the temporal rate of the change in flame front elementary area A:

$$\kappa = \frac{d(\ln A)}{dt} = \frac{1}{A}\frac{dA}{dt}$$

In the spherical propagating flame, the flame stretch is defined as Eq. (3):

$$\kappa = \frac{1}{A}\frac{dA}{dt} = \frac{1}{4\pi R^2}\frac{d(4\pi R^2)}{dt} = \frac{2}{R}\frac{dR}{dt} = \frac{2}{R}S_b$$

There is a linear relationship between the stretched flame propagation speed and flame stretch rate, can be expressed as[23]:

$$S_b = S_b^0 - L_b \kappa , \quad (4)$$

Where S_b^0 - unstretched flame propagation speed, cm/s; L_b - Markstein length, mm; κ - flame stretch rate. The unstretched flame propagation speed can obtained by extrapolating to zero stretch, and the Markstein length is the negative value of the slope of the $S_b - \kappa$ curve. The unstretched laminar flame speed, S_L, was calculated from the mass conservation across the thin flame front, Eq.(2):

$$S_L = \frac{S_b^0}{\sigma} = S_b^0 \frac{\rho_b}{\rho_u} , \quad (5)$$

Where σ - the thermal expansion ratio; ρ_b - the density of the burned mixture, kg/m^3; ρ_u - the density of the unburned mixture, kg/m^3. The quantities ρ_b and ρ_u were calculated using the equilibrium module of CHEMKIN.

3.2 Lewis number

The cellular instability of the premixed mixture is considered causing by diffusive-thermal instability and hydrodynamic instability. The intensity of the diffusive disparity associated with the diffusional-thermal instability can be described using the Lewis number (*Le*). An effective *Le* less than unity indicates that the flame becomes unstable under the diffusional-thermal instability. The Lewis number is the ratio of the thermal diffusivity of the mixture over the mass diffusivity of the deficient species into the diluent:

$$Le = \frac{D_T}{D_M} = \frac{\lambda}{\rho_u C_p D_M} , \quad (6)$$

where D_T - thermal diffusivity coefficient; D_M - the mass diffusivity coefficient; λ - the unburn gas thermal conductivity, (W/(m · K)); C_P - the specific heat at constant pressure, kJ/(kg · K). For the 50%NH_3/50%H_2/air flames, two fuels exist in the reactants, the effective Lewis number (Le_{eff}) in this work used the volume-weighted method to calculate [24]:

$$Le_{eff} = X_{H_2} Le_{H_2} + X_{NH_3} Le_{NH_3} \quad (7)$$

where X_{H_2} - the volume fraction of H_2; X_{NH_3} - the volume fraction of NH_3; Le_{H_2} - the Lewis number of H_2; Le_{NH_3} - the Lewis number of NH_3.

3.3 Thermal expansion ratio and flame thickness

Hydrodynamic instability always exists during the process of flame propagation connected with the expansion of combustion products. Thermal expansion across the flame front and the laminar flame thickness are two important parameters having strong influence on the hydrodynamic instability. The

thermal expansion ratio is shown in Eq. (2). The laminar flame thickness, δ, can be determined by Eq.(5):

$$\delta = \frac{\lambda}{C_P \rho_u S_L}, \tag{8}$$

The hydrodynamic instability is directly proportional to the thermal expansion ratio, σ, and inversely proportional to the flame thickness, δ. The increasing σ and the decreasing δ can strength the hydrodynamic instability [25].

4.0 Result and discussion

4.1 Laminar burning velocity

Figure 2 shows experimental and numerical results of the relationship between laminar burning velocity S_L, and equivalence ratio ϕ, at unburned temperature and pressure of T_u = 298K and P_u = 1 atm, respectively. The laminar velocity reaches its maximum value at the equivalence ratio of 1.1. This tendency is the same to the hydrocarbon fuels, and these values are close to those for methane burning in air under the same conditions. The results obtained experimentally by C. Lhuillier et al. [26], J.H. Lee et al. [12], J. Li et al. [27] are also plotted in Fig. 2. Few data are available for ammonia and hydrogen equivalent combustion, and the data from different studies differs to a considerable extent, especially at the rich side. The result here are more consistent with that of C. Lhuillier [26]. Overall, the measurements of laminar burning velocities are within the reported data. This supports the reliability of the present experiments. The numerical results with different detailed reaction mechanisms show that the calculated laminar burning velocity increases with equivalence ratio and reaches the peak at the equivalence ratio of ϕ = 1.1, as shown Fig. 2. It decreases with the further increasing equivalence ratio. The predicted results with the detailed chemical kinetics except for Nakamura-Mech [19] are close at the lean burn and smaller than the current experimental results. The results from Nakamura-Mech [19] are closer to J. Li et al. [27] at all of the equivalence ratio. The calculated values from Daugaut-Mech [18] and Zhang-Mech [20] are closer to the current experimental results at rich burn. But the results from Mei-Mech [16] and Han-Mech [17] is underestimated to some extent at rich conditions. The reason that the reaction mechanisms used may not be accurate enough for the addition of hydrogen is that these mechanisms have different scopes of application. The Mei-Mech [16] was developed based on the combustion of ammonia under oxygen enrichment. The Han-Mech [17] considers the carbonaceous materials, CO, mainly applied to NH_3/H_2/Air, NH_3/CO/Air, and NH_3/CO/H_2/Air flames. The results of this mechanism can be close to experimental data for NH_3/H_2/Air flame for hydrogen addition less than 40%. The Dagaut-Mech [18] and the Nakamura-Mech [19] focus on the oxidation of HCN and the NH_3/Air weak flames respectively. Zhang-Mech [20] was developed to describe the pyrolysis and oxidation of H_2/NO_X and syngas/NO_X systems.

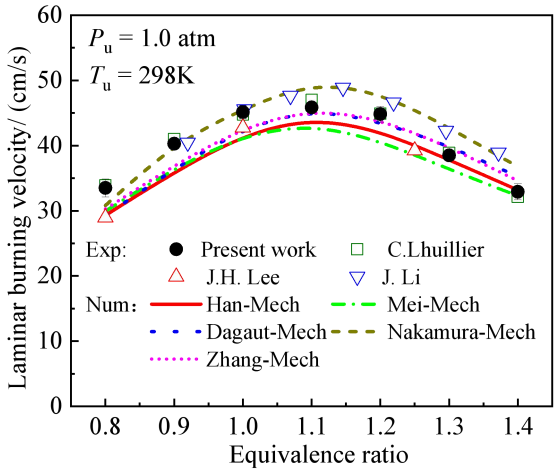

Figure 2. Laminar burning velocity of 50%NH_3/50%H_2/air flames at T_u = 298K, P_u = 1.0 atm. Symbols: experiments. Lines: numerical models.

Figure 3 (a) shows the measured laminar burning velocity of 50%NH_3/50%H_2/air mixtures at T_u = 298K and P_u = 0.5, 1.0 and 1.5 atm. The results show that the laminar burning velocity at same initial pressure increases with the equivalence ratio under the lean burn and decreases with the equivalence ratio under rich burn. At the three initial pressures, the peak values of the measurement appear at equivalence ratio of ϕ = 1.1, and decrease with the increasing initial pressure. This trend is the same as hydrocarbon flames. Fig. 3 (b) shows the measured laminar burning velocity of 50%NH_3/50%H_2/air mixtures at T_u = 298K and equivalence ratio of ϕ = 0.8, 1.0 and 1.3. All of the laminar burning velocities decrease with increasing initial pressure at different equivalence ratios, and the decreasing extent becomes weaker with increasing the initial pressure.

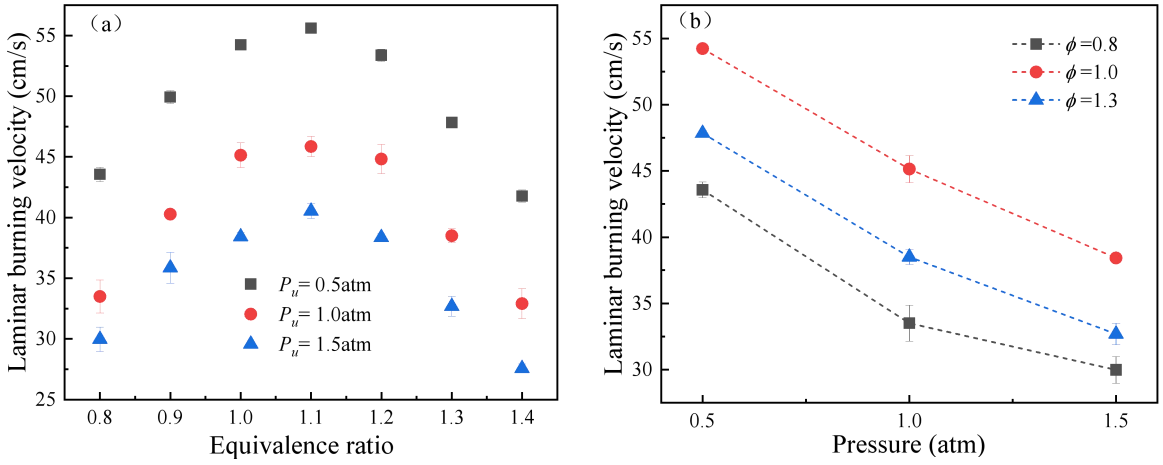

Figure 3. Measured laminar burning velocity of 50%NH_3/50%H_2/air flames at T_u = 298K: (a) as function of equivalence ratio at P_u = 0.5, 1.0 and 1.5 atm, and (b) as function of initial pressure at equivalence ratio of ϕ = 0.8, 1.0 and 1.3.

4.2 Markstein length

The Markstein length is usually used to characterize the sensitivity of flame response to stretching, as defined in Eq. (1). Figure 4 shows the measured Markstein length of 50%NH_3/50%H_2/air flames with

different equivalence ratios at T_u = 298K and P_u = 0.5, 1.0 and 1.5 atm. The Markstein length increases with increasing equivalence ratio for all the same initial pressures. This tendency is the same as the CH_4/air, H_2/air, and NH_3/air flames where the fuel is the lighter component in the combustible mixtures [16]. In general, when the Markstein length is positive, the increase of stretching decreases the flame propagation rate and leads to a stable flame. When the Markstein length is negative, the flame propagation rate increases due to the increasing stretching and an unstable flame develops. For P_u = 1.0 and 1.5atm, the Markstein length is negative at the equivalence ratios less than 1.0, and the flame front has more cracks with decreasing equivalence ratio. The positive Markstein length increases with the increase of equivalence ratio when $\phi > 1.1$, and thus the flame becomes more stable. For the same equivalence ratio, the Markstein length decreases with the increase of initial pressure and the flame becomes more unstable (as will be shown below). This implies that the increase of initial pressure enhances the instability of 50%NH_3/50%H_2/air flames.

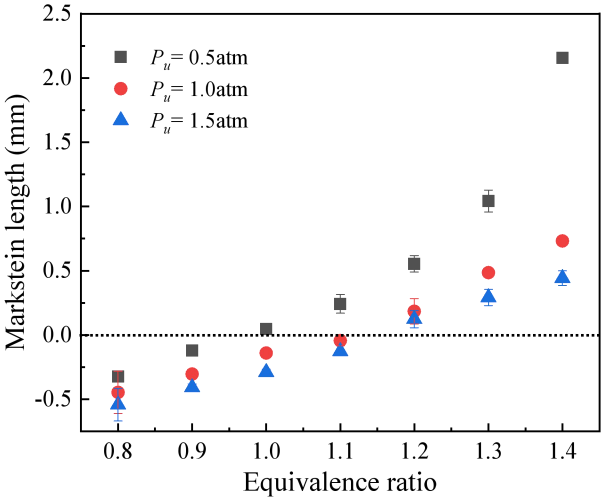

Figure 4. Measured Markstein length of 50%NH_3/50%H_2/air flames at T_u = 298K and P_u = 0.5, 1.0 and 1.5 atm.

4.3 Flame instability

4.3.1 Effect of equivalence ratio

Figure 5 shows the effective Lewis number, thermal expansion ratio and flame thickness change with equivalence ratio at P_u =1.0 atm. Effective Lewis number is negative at the equivalence ratio of $\phi <$ 1.0, but positive at the equivalence ratio of $\phi >$ 1.0. This indicates that the diffusional-thermal instability can destabilize the surface of flame under lean burn and stabilize the flame under rich burn. The thermal expansion ratio increases with equivalence ratio firstly and reaches the peak at ϕ = 1.05, then decreases with equivalence ratio. The trend of flame thickness is opposite to that of thermal expansion ratio. This indicates that the hydrodynamic instability is enhanced under lean burn and weakened under rich burn with increasing equivalence ratio.

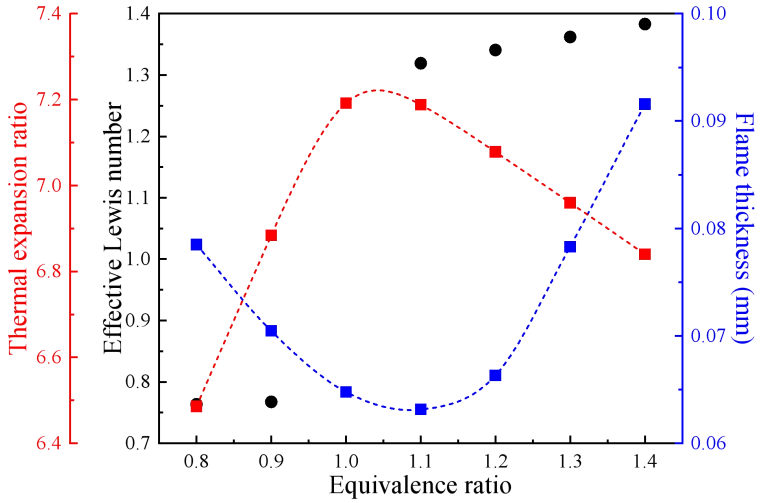

Figure 5. Effective Lewis number, thermal expansion ratio and flame thickness as a function of equivalence ratio (ϕ = 0.8-1.3) at T_u = 298K, P_u = 1.0 atm.

Figure 6 shows a temporal sequence of schlieren images of cracked flame front under lean burn at P_u=1.0 atm. While the flame is stable under stoichiometric and rich burn, it becomes stable with increasing equivalence ratio but the most wrinkle flame does not appear at the equivalence ratio of ϕ = 1.0. From the above, it is known that the combination of the diffusional-thermal instability and hydrodynamic instability lead to the development of cellular structures under lean burn. Nevertheless, the effect of the diffusional-thermal instability is more important.

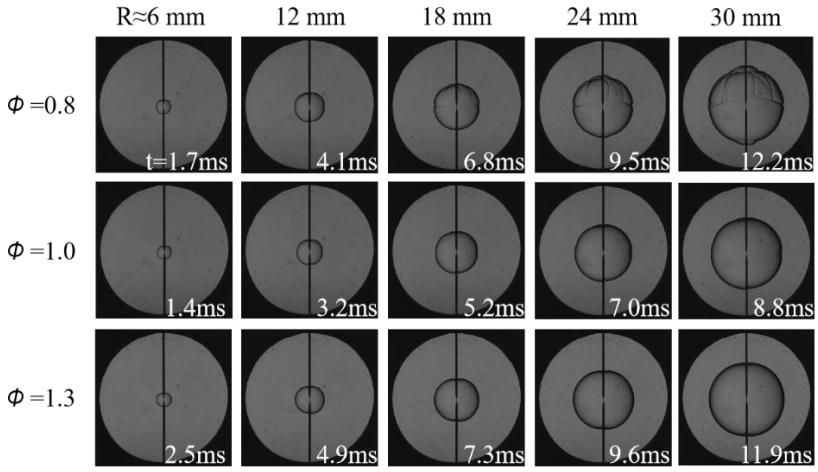

Figure 6. Schlieren images of spherically propagating 50%NH_3/50%H_2/air flames at P_u = 1.0 atm, T_u = 298 K and ϕ = 0.8, 1.0 and 1.3.

4.3.2 Effect of pressure

Figure 7 shows the effective Lewis number, thermal expansion ratio and flame thickness as a function of initial pressure. The effective Lewis number almost keeps constant with increasing initial pressure for a specific equivalence ratio, as shown in Fig. 7(a). This implies that the diffusional-thermal instability is insensitive to the change of initial pressure. The trend of thermal expansion ratio with

increasing initial pressure is the same as that of effective Lewis number, as shown in Fig. 7 (b). This means that the variation of initial pressure can hardly cause a significant difference of the thermal expansion effect. Different from the tendency of thermal expansion ratio, the flame thickness changes obviously with increasing initial pressure. The increase of initial pressure gives rise to a monotonous decreases of the flame thickness for a specific equivalence ratio, as shown in Fig. 7(c). The thinning flame thickness weakens the influence of curvature and strengthens the baroclinic torque intensity of the flame front, and thus enhances the hydrodynamic instability.

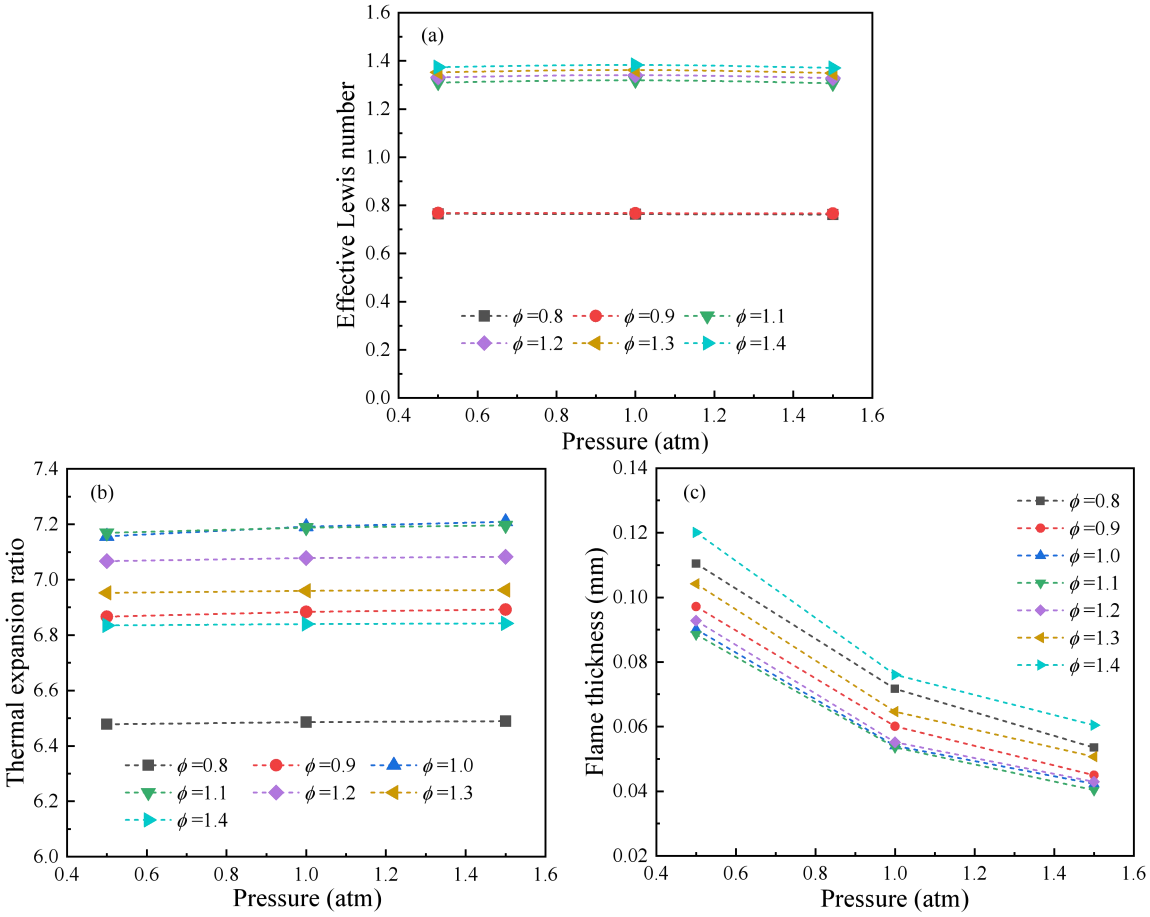

Figure 7. The influence parameters of instability change with different initial pressures (P_u = 0.5-1.5) at T_u = 298K. (a): Effective Lewis number. (b): Thermal expansion ratio. (c): Flame thickness.

Figure 8 shows a sequence of schlieren images of spherically propagating 50%NH3/50%H2/air flames at R ≈ 30 mm, T_u = 298 K, P_u = 0.5-1.5atm, and ϕ = 0.8-1.3. The flame front is smooth at P_u = 0.5 atm within the equivalence ratio of ϕ = 0.8-1.3, as shown in Fig. 8. There are a few wrinkles appearing on the flame surface when the initial pressure increases to P_u = 1.0 atm for lean burn, and more wrinkles are observed at a higher pressure of P_u = 1.5 atm. Therefore, the flame becomes more unstable with increasing initial pressure.

The above results show that an increase in initial pressure leads to slight changes in effective Lewis number and thermal expansion ratio. This means that the flames in the mixtures at ϕ = 0.8-1.3 are diffusively stable with the increase of initial pressure. However, an increase in initial pressure is favourable for hydrodynamic instability since it results in a significant decrease in flame thickness.

Therefore, the cellular instabilities of 50%NH_3/50%H_2/air flames with increasing initial pressure are mainly attributed to the hydrodynamic instability. The regular folds of the cellular flames also manifest this nature.

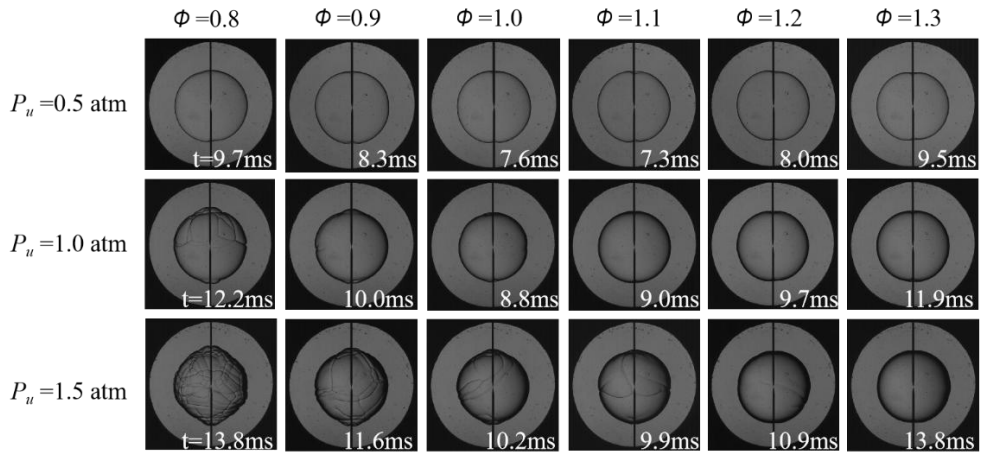

Figure 8. Schlieren images of spherical 50%NH_3/50%H_2/air flames at R ≈ 30 mm, T_u = 298K, P_u = 0.5-1.5 atm, and ϕ = 0.8-1.3.

5.0 CONCLUSIONS

The effect of elevated pressures on laminar burning velocity, Markstein length and cellular instabilities of spherically propagating 50%NH_3/50%H_2/air premixed flames were investigated at different equivalence ratios. The major conclusions of this study are as follows:

(1) The unstretched laminar burning velocity reaches the peak at the equivalence ratio of ϕ =1.1 and decreases with increasing initial pressure. The results of numerical simulations using different chemical kinetics except for Nakamura-Mech are smaller than the experimental measurements at lean burn, but the predictions by Dagaut-Mech and Zhang-Mech are consistent with the current experimental data at rich burn.

(2) Measured Markstein length of 50%NH_3/50%H_2/air flames increases monotonically with the increase of equivalence ratio, leading to a more stabilized flame. On the contrary, increasing initial pressure leads to a decreasing Markstein length and thus results in a more unstable flame.

(3) Both the diffusional-thermal and hydrodynamic instabilities are intensified with the increasing equivalence ratio, although the cellular structure on the lean flame surface is mainly attributed to the diffusional-thermal instability. The increase of initial pressure causes increasingly, unstable cellular flames for the 50%NH_3/50%H_2/air mixture due to the hydrodynamic instability.

REFERENCES

1. Chiuta, S., Everson, R.C., Neomagus, H.W.J.P., van der Gryp, P. and Bessarabov, D.G., Reactor technology options for distributed hydrogen generation via ammonia decomposition: A review, *International Journal of Hydrogen Energy*, **38**, No. 35, 2013, pp. 14968-14991.

2. Han, X.L., Wang, Z.H., He, Y., Zhu, Y.Q. and Cen, K.F., Experimental and kinetic modeling study of laminar burning velocities of NH3/syngas/air premixed flames, *Combustion and Flame*, **213**, No. 2020, pp. 1-13.
3. Kurata, O., Iki, N., Matsunuma, T., Inoue, T., Tsujimura, T., Furutani, H., Kobayashi, H. and Hayakawa, A., Performances and emission characteristics of NH3–air and NH3CH4–air combustion gas-turbine power generations, *Proceedings of the Combustion Institute*, **36**, No. 3, 2017, pp. 3351-3359.
4. Ryu, K., Zacharakis-Jutz, G.E. and Kong, S.-C., Performance enhancement of ammonia-fueled engine by using dissociation catalyst for hydrogen generation, *International Journal of Hydrogen Energy*, **39**, No. 5, 2014, pp. 2390-2398.
5. Afif, A., Radenahmad, N., Cheok, Q., Shams, S., Kim, J.H. and Azad, A.K., Ammonia-fed fuel cells: a comprehensive review, *Renewable and Sustainable Energy Reviews*, **60**, No. 2016, pp. 822-835.
6. Ciccarelli, G., Jackson, D. and Verreault, J., Flammability limits of NH3–H2–N2–air mixtures at elevated initial temperatures, *Combustion and Flame*, **144**, No. 1-2, 2006, pp. 53-63.
7. Cui, G., Li, Z. and Yang, C., Experimental study of flammability limits of methane/air mixtures at low temperatures and elevated pressures, *Fuel*, **181**, No. 2016, pp. 1074-1080.
8. Hayakawa, A., Goto, T., Mimoto, R., Arakawa, Y., Kudo, T. and Kobayashi, H., Laminar burning velocity and Markstein length of ammonia/air premixed flames at various pressures, *Fuel*, **159**, No. 2015, pp. 98-106.
9. Kim, H.J., Van, K., Lee, D.K., Yoo, C.S., Park, J. and Chung, S.H., Laminar flame speed, Markstein length, and cellular instability for spherically propagating methane/ethylene–air premixed flames, *Combustion and Flame*, **214**, No. 2020, pp. 464-474.
10. Okafor, E.C., Naito, Y., Colson, S., Ichikawa, A., Kudo, T., Hayakawa, A. and Kobayashi, H., Experimental and numerical study of the laminar burning velocity of CH4–NH3–air premixed flames, *Combustion and Flame*, **187**, No. 2018, pp. 185-198.
11. Gross, C.W. and Kong, S.-C., Performance characteristics of a compression-ignition engine using direct-injection ammonia–DME mixtures, *Fuel*, **103**, No. 2013, pp. 1069-1079.
12. Lee, J.H., Kim, J.H., Park, J.H. and Kwon, O.C., Studies on properties of laminar premixed hydrogen-added ammonia/air flames for hydrogen production, *International Journal of Hydrogen Energy*, **35**, No. 3, 2010, pp. 1054-1064.
13. Ichikawa, A., Hayakawa, A., Kitagawa, Y., Kunkuma Amila Somarathne, K.D., Kudo, T. and Kobayashi, H., Laminar burning velocity and Markstein length of ammonia/hydrogen/air premixed flames at elevated pressures, *International Journal of Hydrogen Energy*, **40**, No. 30, 2015, pp. 9570-9578.
14. Li, J., Huang, H., Kobayashi, N., Wang, C. and Yuan, H., Numerical study on laminar burning velocity and ignition delay time of ammonia flame with hydrogen addition, *Energy*, **126**, No. 2017, pp. 796-809.
16. Mei, B.W., Zhang, X.Y., Ma, S.Y., Cui, M.L., Guo, H.W., Cao, Z.H. and Li, Y.Y., Experimental and kinetic modeling investigation on the laminar flame propagation of ammonia under oxygen enrichment and elevated pressure conditions, *Combustion and Flame*, **210**, No. 2019, pp. 236-246.
17. Han, X., Wang, Z., Costa, M., Sun, Z., He, Y. and Cen, K., Experimental and kinetic modeling study of laminar burning velocities of NH3/air, NH3/H2/air, NH3/CO/air and NH3/CH4/air premixed flames, *Combustion and Flame*, **206**, No. 2019, pp. 214-226.

18. Dagaut, P., Glarborg, P. and Alzueta, M., The oxidation of hydrogen cyanide and related chemistry, *Progress in Energy and Combustion Science*, **34**, No. 1, 2008, pp. 1-46.
19. Nakamura, H., Hasegawa, S. and Tezuka, T., Kinetic modeling of ammonia/air weak flames in a micro flow reactor with a controlled temperature profile, *Combustion and Flame*, **185**, No. 2017, pp. 16-27.
20. Zhang, Y., Mathieu, O., Petersen, E.L., Bourque, G. and Curran, H.J., Assessing the predictions of a NO x kinetic mechanism on recent hydrogen and syngas experimental data, *Combustion and Flame*, **182**, No. 2017, pp. 122-141.
21. Kelley, A.P. and Law, C.K., Nonlinear effects in the extraction of laminar flame speeds from expanding spherical flames, *Combustion and Flame*, **156**, No. 9, 2009, pp. 1844-1851.
22. Burke, M.P., Chen, Z., Ju, Y. and Dryer, F.L., Effect of cylindrical confinement on the determination of laminar flame speeds using outwardly propagating flames, *Combustion and Flame*, **156**, No. 4, 2009, pp. 771-779.
23. Bradley, D., Hicks, R.A., Lawes, M., Sheppard, C.G.W. and Woolley, R., The measurement of laminar burning velocities and Markstein numbers for Iso-octane–air and Iso-octane–n-Heptane–air mixtures at elevated temperatures and pressures in an explosion bomb, *Combustion and Flame*, **115**, No. 1998, pp. 126-144.
24. Bouvet, N., Halter, F., Chauveau, C. and Yoon, Y., On the effective Lewis number formulations for lean hydrogen/hydrocarbon/air mixtures, *International Journal of Hydrogen Energy*, **38**, No. 14, 2013, pp. 5949-5960.
25. Kwon, O.C., Rozenchan, G. and Law, C.K., Cellular instabilities and self-acceleration of outwardly propagating spherical flames, *proceedings of the combustion institute*, **29**, No. 2002, pp. 1775-1783.
26. Lhuillier, C., Brequigny, P., Lamoureux, N., Contino, F. and Mounaïm-Rousselle, C., Experimental investigation on laminar burning velocities of ammonia/hydrogen/air mixtures at elevated temperatures, *Fuel*, **263**, No. 2020.
27. Li, J., Huang, H., Kobayashi, N., He, Z. and Nagai, Y., Study on using hydrogen and ammonia as fuels: Combustion characteristics and NOxformation, *International Journal of Energy Research*, **38**, No. 9, 2014, pp. 1214-1223.

Uncategorized References

15. **Year:** 2016

Title: CHEMKIN-PRO 17.0 Release 15151

Publisher: Reaction Design

Short Title: CHEMKIN-PRO 17.0 Release 15151